J. Fluid Mech. (1990), *vol.* 210, *pp.* 281–302
Printed in Great Britain

Steady two-dimensional flow through a row of normal flat plates

By D. B. INGHAM[1], T. TANG[1] AND B. R. MORTON[2]

[1] Department of Applied Mathematical Studies, University of Leeds, Leeds LS2 9JT, UK

[2] Department of Mathematics, Monash University, Clayton, Victoria, 3168, Australia

(Received 5 August 1988 and in revised form 27 June 1989)

A numerical and experimental study is described for the two-dimensional steady flow through a uniform cascade of normal flat plates. The Navier–Stokes equations are written in terms of the stream function and vorticity and are solved using a second-order-accurate finite-difference scheme which is based on a modified procedure to preserve accuracy and iterative convergence at higher Reynolds numbers. The upstream and downstream boundary conditions are discussed and an asymptotic solution is employed both upstream and downstream. A frequently used method for dealing with corner singularities is shown to be inaccurate and a method for overcoming this problem is described. Numerical solutions have been obtained for blockage ratio of 50% and Reynolds numbers in the range $0 \leqslant R \leqslant 500$ and results for both the lengths of attached eddies and the drag coefficients are presented. The calculations indicate that the eddy length increases linearly with R, at least up to $R = 500$, and that the multiplicative constant is in very good agreement with the theoretical prediction of Smith (1985*a*), who considered a related problem. In the case of $R = 0$ the Navier–Stokes equations are solved using the finite-difference scheme and a modification of the boundary-element method which treats the corner singularities. The solutions obtained by the two methods are compared and the results are shown to be in good agreement. An experimental investigation has been performed at small and moderate values of the Reynolds numbers and there is excellent agreement with the numerical results both for flow streamlines and eddy lengths.

1. Introduction

The problem of steady viscous incompressible flow past bluff bodies has over a long time received much attention, both theoretically and numerically. In spite of the many numerical methods and calculations on flow past a circular cylinder, accurate results have been obtained only for Reynolds number $R(= Ud/\nu$, where U is the uniform speed relative to the cylinder at large distance, d the diameter of the cylinder and ν the kinematic viscosity of the fluid) up to about 600, see Fornberg (1985). He found that the wake bubble (region of attached or recirculating flow) has eddy length $L \propto R$, with width $W \propto R^{\frac{1}{2}}$ up to $R = 300$ and beyond that $W \propto R$. Smith (1979) developed an asymptotic theory which is based on an extension of Kirchhoff's (1869) free-streamline solution which agrees with Fornberg's results up to $R \approx 300$ only, and Smith (1985*b*) and Peregrine (1985) have performed theoretical work which gives a fresh interpretation of Fornberg's results. There are several differences between the theories of Smith and Peregrine, some of which are a matter of interpretation, and these are unlikely to be resolved without further analysis and computational work.

Hudson & Dennis (1985) investigated numerical solutions of the Navier–Stokes equations for steady laminar flow of a viscous incompressible fluid past a normal flat plate rather than a circular cylinder. They were able to obtain accurate numerical results for R up to 20 only because of the difficulty in resolving the singularity at the edges of the plate. Their results for the eddy length were in excellent agreement with the observations of Prandtl & Tietjens (1934) and Acrivos *et al.* (1968). However, although the eddy length grows linearly in agreement with Smith (1979, 1985*b*) and Peregrine (1985), the constants of proportionality are significantly different. Castro, Cliffe & Norgett (1982) and Castro & Jones (1987) have investigated the steady laminar flow in a channel past a normal flat plate with a downstream splitter plate, for a blockage ratio of 20%, and found that the bubble length increases linearly with the Reynolds number, up to $R = 500$. Acrivos *et al.* (1968) performed experiments on flow past a variety of isolated bluff bodies and confirmed that the length of the recirculating bubble increases linearly with the Reynolds number. However, they reported also that the widths of their bubbles attained a limit $O(1)$ as R increases, in accordance with the earlier predictions of Acrivos *et al.* (1965). This result has been disputed by Smith (1979, 1985*b*), Fornberg (1980, 1985), and Peregrine (1985), all of whom suggest that the width increases as R increases.

In a series of papers Acrivos & Schrader (1982), Milos & Acrivos (1986) and Milos, Acrivos & Kim (1987) have studied the related problem of laminar flow over a backward-facing step on one side of a two-dimensional channel. They have studied both the boundary-layer equations and the full Navier–Stokes equations; with entry profiles which are parabolic, uniform, and one that simulates uniform flow over a boundary layer shed from the step, and results have been obtained over a wide range of values of λ, the ratio of the upstream channel half-width to the step height. The general conclusion they reach is that steady solutions are not always possible. Where they are, the eddy length increases with R for small values of λ but for large values of λ the limit with increasing R for the non-dimensional length of eddy is $O(1)$. Smith (1985*a*) studied this problem both theoretically and numerically and found that for all blockage ratios the length of the wake bubble continued to increase with R.

Although some agreement between theoretical, numerical and experimental results exists, there is a need for further work in all these aspects of this fundamental and classical problem. In this paper we investigate the flow of a uniform stream past a geometrically simple cascade consisting of an infinite array of identical flat plates of finite width which are normal to the flow direction. The steady-state Navier–Stokes equations are solved using a finite-difference technique in an infinite region with boundary conditions of uniform flow being applied at infinity in both the upstream and downstream directions. It should be noted particularly that in most previous numerical work the boundary conditions have been applied at the station where the flow leaves the cascade and at large distance downstream, and that the flow leaving the cascade has been assumed to be: (i) parabolic, (ii) uniform, or (iii) uniform above a simulated boundary layer of specified thickness discharging over the step. These models do no more than approximate the physical problem of a uniform upstream flow passing through a cascade, and in this paper we illustrate some of their inadequacies.

The fluid flow through a cascade of bluff bodies is of fundamental importance for two reasons. First, the resultant predictions relate to the performance of the cascade itself, providing a model for flow past compressor and turbine blades, for many types of heat exchanger and for other interactive body configurations. In practice, the attached flow behind the cascade may have severe consequences for heat transfer and

drag, and an understanding of the flow and of the dependence of bubble lengths on Reynolds number is of immediate concern. Secondly, the cascade configuration provides valuable insight into quite fundamental properties of flow. The main properties are attained when the cascade becomes widely spaced. Smith (1985*a*) established a theoretical basis for understanding the separated flow structure produced by the cascade configuration and there is special interest in relating experimental and numerical studies to his theory.

In a numerical treatment of flow past a cascade of normal plates, difficulties arise in applying boundary conditions near the plate edges. The problem has been discussed in detail by several authors (see Fornberg 1980; Dennis & Hudson 1980; and Ingham 1983). The sudden discontinuity in conditions near the edge of the plate gives rise to a singularity in the vorticity and this is handled in our treatment by using the appropriate form of the analytical solution in this vicinity following Moffatt (1964). In dealing with the corner singularity a method which has been frequently used is shown to be inaccurate. It is very important that the solution in the vicinity of the singularity is accurately obtained as errors introduced are swept downstream and may severely affect such quantities as the length of the attached eddies. Also, we adopt asymptotic solutions both upstream and downstream so that the numerical integrations need be carried out over a finite region only. We have obtained numerical solutions in the range $0 \leqslant R \leqslant 500$ for the cascade with 50% blockage ratio in which plate and gap widths are equal.

When the Reynolds number of the flow is zero, the equations of motion reduce to the biharmonic equation. This has been solved using a modification of the boundary-element method which treats the corner singularities. The finite-difference and boundary-element solutions are compared and the results shown to be in good agreement.

An experimental investigation has been performed for flow through a cascade of normal flat plates with equal plate and gap widths. At small and moderate values of the Reynolds numbers the flow is symmetrical and the experimental results compare well with the present numerical predictions and the theoretical results of Smith (1985*a*) who considered a related problem.

2. Basic equations

The cascade is assumed to consist of an infinite number of flat plates which are of infinitesimal thickness in the X-direction, of uniform width $2H_{\mathrm{W}}$ in the Y-direction and of infinite extend in the Z-direction. The plates occupy the plane $X = 0$ with edges at $Y = H_{\mathrm{W}} + 2nH_{\mathrm{C}}$ and $Y = -H_{\mathrm{W}} + 2nH_{\mathrm{C}}$, where $n = 0, \pm 1, \pm 2, \ldots$; H_{W} and H_{C} are the half-widths of plate and plate plus gap, respectively (see figure 1). At large distances from the cascade the fluid is assumed to be moving with constant speed U in the positive X-direction and because of symmetry in the Y-direction we need consider only two-dimensional flow in the region $-\infty < X < \infty$, $0 \leqslant Y \leqslant H_{\mathrm{C}}$. In terms of the non-dimensional coordinates $x = X/H_{\mathrm{W}}$ and $y = Y/H_{\mathrm{W}}$, the stream function ψ and vorticity ω satisfy

$$u = \frac{\partial \psi}{\partial y}, \quad v = -\frac{\partial \psi}{\partial x}, \tag{2.1}$$

$$\omega = \frac{\partial v}{\partial x} - \frac{\partial u}{\partial y}; \tag{2.2}$$

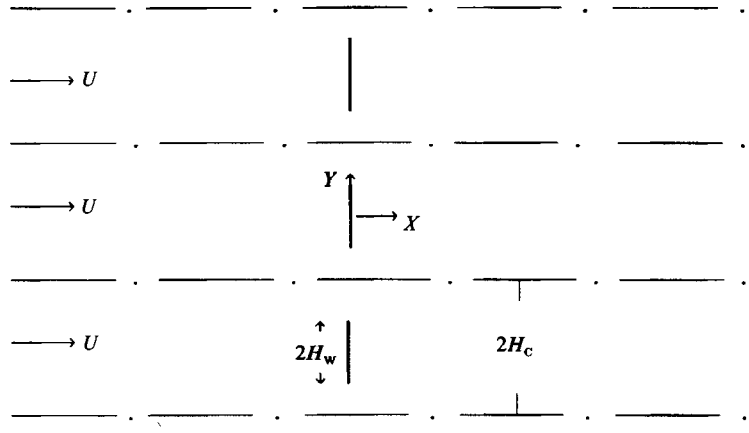

FIGURE 1. The overall cascade flow structure.

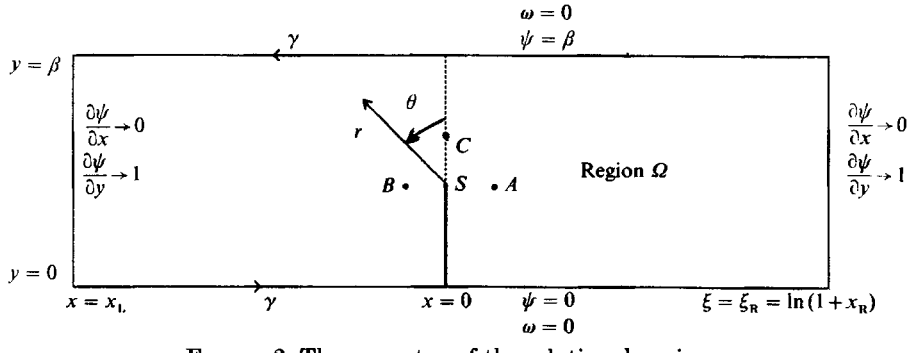

FIGURE 2. The geometry of the solution domain.

and the Navier–Stokes equations take the non-dimensional form

$$\nabla^2\psi = -\omega, \tag{2.3a}$$

$$\nabla^2\omega = \tfrac{1}{2}R\left(\frac{\partial\psi}{\partial y}\frac{\partial\omega}{\partial x} - \frac{\partial\psi}{\partial x}\frac{\partial\omega}{\partial y}\right), \tag{2.3b}$$

where $R = 2H_{\mathrm{w}}U/\nu$ is the Reynolds number, ν kinematic viscosity, and all lengths, velocities and pressure have been non-dimensionalised with respect to H_{w}, U and ρU^2 respectively, where ρ is the fluid density assumed constant. The boundary conditions (see figure 2) are

$$\frac{\partial\psi}{\partial y} = 0, \quad \frac{\partial\psi}{\partial x} = 0 \quad \text{on} \quad x = 0-, \quad \text{and} \quad x = 0+, \quad 0 \leqslant y \leqslant 1, \tag{2.4}$$

$$\frac{\partial\psi}{\partial y} \to 1, \quad \frac{\partial\psi}{\partial x} \to 0 \quad \text{as} \quad x \to \infty, \quad 0 \leqslant y \leqslant \beta, \tag{2.5a}$$

$$\frac{\partial\psi}{\partial y} \to 1, \quad \frac{\partial\psi}{\partial x} \to 0 \quad \text{as} \quad x \to -\infty, \quad 0 \leqslant y \leqslant \beta, \tag{2.5b}$$

$$\psi = 0, \quad \omega = 0 \quad \text{on} \quad y = 0, \quad -\infty < x < \infty, \tag{2.6a}$$

$$\psi = \beta, \quad \omega = 0 \quad \text{on} \quad y = \beta, \quad -\infty < x < \infty, \tag{2.6b}$$

where $\beta = H_C/H_W$, and $0-$ and $0+$ represent the left- and right-hand sides of the plate, respectively.

For viable computation we must limit the length (say, $x_L \leqslant x \leqslant x_R$) of the computational region without introducing significant error into the computed length of the attached eddies. As the Reynolds number is increased the attached eddy behind a plate grows in length, and the finite value $x = x_R$ at which boundary condition (2.5*a*) may be applied has to be taken at a sufficiently large distance from the plate. Hence we apply the transformation

$$\xi = \ln(1+x), \tag{2.7}$$

for $x > 0$ and the (2.3*a*) and (2.3*b*) become

$$e^{-2\xi}\left(\frac{\partial^2\psi}{\partial\xi^2} - \frac{\partial\psi}{\partial\xi}\right) + \frac{\partial^2\psi}{\partial y^2} = -\omega, \tag{2.8a}$$

$$e^{-2\xi}\left(\frac{\partial^2\omega}{\partial\xi^2} - \frac{\partial\omega}{\partial\xi}\right) + \frac{\partial^2\omega}{\partial y^2} = \tfrac{1}{2}R\,e^{-\xi}\left(\frac{\partial\psi}{\partial y}\frac{\partial\omega}{\partial\xi} - \frac{\partial\psi}{\partial\xi}\frac{\partial\omega}{\partial y}\right), \tag{2.8b}$$

for $\xi > 0$. The elliptic partial differential equations (2.3) and (2.8) are solved using a finite-difference scheme similar to that described by Dennis & Hudson (1978) and Dennis & Smith (1980).

A mesh system is set up with mesh size in the y-direction $k = 1/N$, where N is a predetermined positive integer. In the x-direction the mesh size is $h_R = \xi_R/M$ for $\xi > 0$ and $h_L = e^{h_R} - 1$ for $x < 0$ where $\xi_R (= \ln(1+x_R))$ is the value of ξ at which the infinity boundary condition (2.5*a*) is applied, and M is a positive integer. Thus the mesh size in the x-direction is constant for $x < 0$ and, although variable for $x > 0$, the size of the first mesh in the region $x > 0$ is the same as that in the region $x < 0$. The boundary condition (2.5*b*) is applied at $x_L = -Ph_L$ where P is a predetermined positive integer. Equations (2.3) and (2.8) are put into finite-difference forms for $x < 0$ and $\xi > 0$, respectively.

We determine the vorticity on the plate at points other than the edge by using the method of Woods (1954), which gives

$$\omega_B = -\frac{3\psi_I}{h^2} - \tfrac{1}{2}\omega_I, \tag{2.9}$$

where the subscript I denotes a value at the first internal grid point adjacent to the boundary grid point B and h is the distance between I and B. There are two values of the vorticity at each boundary grid point on the plate, one to the right and one to the left:

$$\omega(0+, y) = -3\psi(h, y)/h^2 - \tfrac{1}{2}\omega(h, y), \quad 0 \leqslant y < 1, \tag{2.10a}$$

$$\omega(0-, y) = -3\psi(-h, y)/h^2 - \tfrac{1}{2}\omega(-h, y), \quad 0 \leqslant y < 1. \tag{2.10b}$$

In order to minimize the size of the domain of integration we use appropriate asymptotic solutions of the Navier–Stokes equations for large positive and negative values of x. Following Wilson (1969) and Bramley & Dennis (1982) we write

$$\psi(x, y) = y + f(y)\,e^{-\alpha x}, \tag{2.11a}$$

$$\omega(x, y) = g(y)\,e^{-\alpha x}. \tag{2.11b}$$

Substituting these expressions into (2.3*a*) and (2.3*b*) and solving them we obtain

$$\alpha = \tfrac{1}{4}[-R - (R^2 + (4n\pi)^2)^{\frac{1}{2}}] = \alpha_n, \quad \text{say, for} \quad x < 0, \quad n \in \mathbb{N} \tag{2.12a}$$

and

$$\alpha = \tfrac{1}{4}[-R+(R^2+(4n\pi)^2)^{\frac{1}{2}}] = \alpha_n^*, \quad \text{say, for} \quad x>0, \quad n\in\mathbb{N} \tag{2.12b}$$

and

$$f(y) = C_n \sin(n\pi y), \tag{2.13a}$$

$$g(y) = \tfrac{1}{2}\alpha R C_n \sin(n\pi y), \tag{2.13b}$$

with C_n a real constant. From (2.12) and (2.13) we deduce that the asymptotic boundary conditions to be employed are

$$\frac{\partial\psi}{\partial x} \sim -\alpha_1(\psi-y), \quad \frac{\partial\omega}{\partial x} \sim -\alpha_1\omega, \quad \text{as} \quad x\to-\infty, \tag{2.14a}$$

$$\frac{\partial\psi}{\partial x} \sim -\alpha_1^*(\psi-y), \quad \frac{\partial\omega}{\partial x} \sim -\alpha_1^*\omega, \quad \text{as} \quad x\to+\infty, \tag{2.14b}$$

where the upstream boundary condition (2.14a) is applied at $x_{\mathrm{L}} = -Ph_{\mathrm{L}}$. In terms of ξ, (2.14b) becomes

$$\frac{\partial\psi}{\partial\xi} \sim -\alpha_1^* e^{\xi}(\psi-y), \quad \frac{\partial\omega}{\partial\xi} \sim -\alpha_1^* e^{\xi}\omega \quad \text{as} \quad \xi\to+\infty, \tag{2.15}$$

and the downstream boundary conditions (2.15) are applied at $\xi = \xi_{\mathrm{R}}$. This is in contrast with Milos *et al.* (1987), who use the condition $\partial^2\psi/\partial x^2 = 0$ as $x\to+\infty$.

One grid point that needs special attention is the edge of the plate (S in figure 2), where the vorticity is singular. We handle this in terms of values at the three neighbouring grid points $A(h,1)$, $B(-h,1)$ and $C(0,1+k)$ so that finite-difference representations of (2.3) and (2.8) do not involve the value of ω at S.

3. Numerical technique

First we find the solution for a given mesh size h and k with the positions of the infinity boundaries at $x=-10$ and $\xi=2$ for Reynolds number zero. This is achieved by writing the governing partial differential equations (2.3) and (2.8) in finite-difference form using the modified central-difference formulation as described by Dennis & Hudson (1978). The choice of the scale and mesh size in the x-direction means that at $x=0$ and $y\geqslant 1$ the mesh is square and hence there are no difficulties encountered in writing down the finite-difference equations on this line. An initial guess for the vorticity and stream function is made at all mesh points at which these quantities are unknown; usually we set these values to be identically zero. We sweep through the discretized region updating first the stream function starting at $y=\beta-k$, $\xi=2-h$ and proceed in the negative x-direction until we reach $x=-10+h$. This process is repeated along the lines $y=\beta-2k, \beta-3k, \ldots, y=k$ and the whole process is repeated for the vorticity except that the points on $x=0$, $0\leqslant y\leqslant 1$ and points $A(h,1)$, $B(-h,1)$ and $C(0,1+k)$ (see figure 2) are omitted from the sweep. The values of the vorticity on $x=0$, $0\leqslant y<1$ are determined using (2.10).

In order to determine the values of the vorticity at points A, B and C we employ two methods. Method I is that described by Dennis & Smith (1980), where they write the vorticity in finite-difference form, for example at the point $C(0,1+k)$ in terms of the vorticity and stream function at points $(0,1+k)$, $(h,1)$, $(-h,1)$, $(h,1+2k)$ and $(-h,1+2k)$ rather than those values at the points $(0,1+k)$, $(h,1+k)$, $(-h,1+k)$, $(0,1)$ and $(0,1+2k)$. The infinite value of vorticity at $(0,1)$ is then avoided. Both Dennis

& Smith (1980) and Bramley & Dennis (1984) have used this technique successfully in dealing with problems involving singularities.

Method II of dealing with the singularity in vorticity incorporates the theory of Moffatt (1964) (see, for example, Holdstein & Paddon 1981; Bramley & Dennis 1984; and Badr *et al.* 1985). Near S, (2.3) reduces to the biharmonic equation, $\nabla^4\psi = 0$, and we look for a solution near S in the form

$$\psi = r^\lambda F(\theta), \tag{3.1}$$

where (r, θ) are polar coordinates as shown in figure 2. The solution of (2.3) which satisfies the boundary conditions (2.4) is

$$\begin{aligned}\psi \sim\ & r^{\frac{3}{2}}(\tfrac{1}{3}A^*\cos\tfrac{3}{2}\theta + A^*\cos\tfrac{1}{2}\theta - B^*\sin\tfrac{3}{2}\theta - B^*\sin\tfrac{1}{2}\theta)\\ & + r^2C^*(1-\cos 2\theta)\\ & + r^{\frac{5}{2}}(-\tfrac{1}{5}D^*\cos\tfrac{5}{2}\theta + D^*\cos\tfrac{1}{2}\theta - E^*\sin\tfrac{5}{2}\theta + E^*\sin\tfrac{1}{2}\theta)\\ & + r^3(-F^*\cos 3\theta + F^*\cos\theta - \tfrac{1}{3}G^*\sin 3\theta + G^*\sin\theta) + \ldots,\end{aligned} \tag{3.2}$$

and therefore

$$\begin{aligned}\omega \sim\ & r^{-\frac{1}{2}}(-2A^*\cos\tfrac{1}{2}\theta + 2B^*\sin\tfrac{1}{2}\theta) - 4C^* + r^{\frac{1}{2}}(-6D^*\cos\tfrac{1}{2}\theta - 6E^*\sin\tfrac{1}{2}\theta)\\ & + r(-8F^*\cos\theta - 8G^*\sin\theta) + \ldots,\end{aligned} \tag{3.3}$$

where A^*, B^*, C^*, D^*, E^*, F^* and G^* are constants to be determined.

When $R = 0$ the flow is symmetrical about $\theta = 0$ and thus the constants B^*, E^*, and G^* in (3.2) and (3.3) are identically zero. Then

$$\begin{aligned}\psi \sim\ & r^{\frac{3}{2}}(\tfrac{1}{3}A^*\cos\tfrac{3}{2}\theta + A^*\cos\tfrac{1}{2}\theta) + r^2C^*(1-\cos 2\theta) + r^{\frac{5}{2}}(-\tfrac{1}{5}D^*\cos\tfrac{5}{2}\theta + D^*\cos\tfrac{1}{2}\theta)\\ & + r^3(-F^*\cos 3\theta + F^*\cos\theta) + \ldots,\end{aligned} \tag{3.4}$$

$$\omega \sim -2A^*r^{-\frac{1}{2}}\cos\tfrac{1}{2}\theta - 4C^* - 6D^*r^{\frac{1}{2}}\cos\tfrac{1}{2}\theta - 8F^*r\cos\theta + \ldots, \tag{3.5}$$

and we note that the first and third terms of (3.5) are identically zero on the plate and hence the vorticity is finite on the plate.

We have employed several different techniques in order to find the constants A^*, C^* in (3.4) and (3.5) but found the following method to lead to the quickest convergence as the mesh size tends to zero. We determine A^* and C^* for $R = 0$ from values of the stream function at $(0, 1+k)$ and vorticity at $(0, 1-k)$. We then determine from (3.5) the vorticity at the points $(h, 1)$, $(-h, 1)$ and $(0, 1+k)$. On the plate, (3.5) gives

$$\omega \sim -4C^* + 8F^*r + \ldots; \tag{3.6}$$

hence

$$\omega(0, 1) = 2\omega(0, 1-k) - \omega(0, 1-2k). \tag{3.7}$$

Having now obtained an update of all the vorticity and stream-function values, another complete sweep is made in exactly the same way as that described above and this is continued until convergence is achieved. It is found that although the numerical scheme is diagonally dominant, the vorticity on the boundary has to be under-relaxed (≈ 0.2) in order to obtain a convergent solution; but an over-relaxation factor (≈ 1.2) has been used for both vorticity and stream function in the interior of the computational domain.

Having obtained a convergent solution for $R = 0$ with specified mesh sizes h and k, the positions of the infinity boundary conditions are varied until they are considered to be sufficiently far away from the cascade as described in §6. This procedure was repeated for several values of the mesh size h and k.

Once a convergent result had been obtained for a fixed mesh size at $R = 0$ the results at $R = 1$ were obtained using as a first guess the results from $R = 0$. In this case, however, the singularity must be dealt with slightly differently by method II, because the flow is no longer symmetrical about $x = 0$. We take the first three non-zero values of the constants in (3.2) and (3.3), namely A^*, B^* and C^*, and determine these from the knowledge of the stream function at the point $(0, 1+k)$ and vorticity at $(0-, 1-k)$ and $(0+, 1-k)$. On the plate, (3.5) gives

$$\omega(0-, y) \sim 2B^* r^{-\frac{1}{2}} - 4C^*, \tag{3.8}$$

$$\omega(0+, y) \sim -2B^* r^{-\frac{1}{2}} - 4C^*, \tag{3.9}$$

leading as $y \to 1-$ to

$$\omega(0-, y) = 3.25725\,\omega(0-, y-k) - 2.25725\,\omega(0-, y-2k), \tag{3.10}$$

$$\omega(0+, y) = 3.25725\,\omega(0+, y-k) - 2.25725\,\omega(0+, y-2k). \tag{3.11}$$

Having obtained convergent results for $R = 1$, numerical results were obtained for $R = 5$, 10, 20, 50, 100, 200 and 500. Convergence is tested in each case by evaluating

$$\sigma = \Sigma |1 - \omega_0^{(m+1)}/\omega_0^{(m)}|,$$

where summation is over all grid points and the superscripts refer to the number of iterations. When σ is below some pre-assigned tolerance, ϵ, the process is taken as convergent. The value of ϵ was varied but 10^{-4} was found to be sufficiently small for the results presented in this paper to be correct to the number of decimal places quoted. Further, the boundary conditions (2.14a) and (2.15) were initially satisfied at predetermined positions x_L and x_R ($= e^{\xi_R} - 1$), respectively; the magnitudes of x_L and x_R were then increased until there was no significant change in the solution near the plates. It was found that x_L and x_R should be roughly the same at small values of the Reynolds number, whereas x_L can be taken much smaller than x_R at high values of the Reynolds number in order to obtain accurate numerical results.

4. Boundary-element-method solution for $R = 0$

In order to check the finite-difference scheme a boundary-element method (BEM) solution was obtained for $R = 0$. In this case (2.3) reduces to the biharmonic equation,

$$\nabla^4 \psi = 0, \tag{4.1}$$

which can be solved using Green's second theorem with ψ replaced by $\nabla^2\psi$,

$$\int_\gamma [\psi(\nabla^2\phi)' - \psi'\nabla^2\phi]\,d\gamma = \int_\Omega [\psi\nabla^4\phi - \nabla^2\psi\nabla^2\phi]\,d\Omega, \tag{4.2}$$

where a prime indicates differentiation with respect to the unit outward normal, ψ satisfies (4.1), ϕ is an arbitrary function, γ represents the boundary contour, and Ω the surface enclosed by γ, see figure 2. The functions ψ and ϕ can be transposed to give

$$\int_\gamma [\phi(\nabla^2\psi)' - \phi'\nabla^2\psi]\,d\gamma = \int_\Omega [\phi\nabla^4\psi - \nabla^2\phi\nabla^2\psi]\,d\Omega. \tag{4.3}$$

Subtraction of (4.3) from (4.2) gives

$$\int_\gamma [\psi(\nabla^2\phi)' - \psi'\nabla^2\phi + \nabla^2\psi\phi' - (\nabla^2\psi)'\phi]\,d\gamma = \int_\Omega [\psi\nabla^4\phi - \phi\nabla^4\psi]\,d\Omega. \tag{4.4}$$

Choosing ψ to satisfy

$$\nabla^4\psi(\boldsymbol{b}) = \delta(\boldsymbol{a}-\boldsymbol{b}), \tag{4.5}$$

where $\boldsymbol{a}$ is the point in Ω at which ψ is to be evaluated, $\boldsymbol{b}$ a variable point in Ω, and $\delta(\boldsymbol{a}-\boldsymbol{b})$ the three-dimensional Dirac delta function, gives

$$\int_\Omega [\psi(\nabla^2\phi) - \psi'(\nabla^2\phi) + \nabla^2\psi\phi' - (\nabla^2\psi)'\phi]\,\mathrm{d}\Omega = \sigma(\boldsymbol{a})\,\psi(\boldsymbol{b}), \tag{4.6a}$$

where $\sigma(\boldsymbol{a})$ is a space function which takes the following values:

$$\left.\begin{aligned} &\sigma(\boldsymbol{a}) = 2\pi && \text{if} \quad \boldsymbol{a}\in\Omega-\gamma, \\ &\sigma(\boldsymbol{a}) = \pi && \text{if} \quad \boldsymbol{a}\in\gamma, \quad \gamma \text{ continuous at } \boldsymbol{a}, \\ &\sigma(\boldsymbol{a}) = \text{'internal angle'} && \text{if} \quad \boldsymbol{a}\in\gamma, \quad \gamma \text{ discontinuous at } \boldsymbol{a}. \end{aligned}\right\} \tag{4.6b}$$

Equation (4.6) yields the fundamental solution for the biharmonic equation

$$\phi(|\boldsymbol{a}-\boldsymbol{b}|) = \tfrac{1}{4}(\boldsymbol{a}-\boldsymbol{b})^2\{\log(|a-b|)-1\}. \tag{4.7}$$

It remains only to find all the values of ψ and its derivatives on the boundary, γ, in order to calculate ψ anywhere in Ω. Employing numerical techniques yields a series of equations which are successive approximations to (4.6a). Discretizing the boundary into n straight line elements, γ_j, and approximating the stream function and its derivatives by piecewise smooth constant functions yields

$$\sum_{j=1}^{n}\int_{\gamma_j} [\psi_j(\nabla^2\phi)' - \psi_j'(\nabla^2\phi) - w_j\phi' + \omega_j'\phi]\,\mathrm{d}\gamma = \sigma(\boldsymbol{a})\,\psi(\boldsymbol{a}), \tag{4.8}$$

where ψ_j, ψ_j', ω_j and ω_j' represent the approximations to ψ, ψ', ω and ω' on the element j. If $\boldsymbol{a}$ is now chosen in turn to be the midpoint of each element γ_i, we obtain,

$$\sum_{i=1}^{n}\sum_{j=1}^{n} (\psi_j J_{ij} - \psi_j' K_{ij} - \omega_j L_{ij} + \omega_j' M_{ij}) = 0, \tag{4.9}$$

where

$$J_{ij} = \int_{\gamma_j} \nabla^2\phi'(q_i,\gamma_j)\,\mathrm{d}\gamma - \delta_{ij}\sigma_i\psi_j, \tag{4.10a}$$

$$K_{ij} = \int_{\gamma_j} \nabla^2\phi(q_i,\gamma_j)\,\mathrm{d}\gamma, \tag{4.10b}$$

$$L_{ij} = \int_{\gamma_j} \phi'(q_i,\gamma_j)\,\mathrm{d}\gamma, \tag{4.10c}$$

$$M_{ij} = \int_{\gamma_j} \phi(q_i,\gamma_j)\,\mathrm{d}\gamma, \tag{4.10d}$$

where δ_{ij} is the Kronecker delta, q_i is the midpoint of element i. Equation (4.9) can be re-expressed, in matrix form, as

$$\boldsymbol{J\psi} + \boldsymbol{K\psi'} + \boldsymbol{L\omega} + \boldsymbol{M\omega'} = \boldsymbol{0}, \tag{4.11}$$

where $\boldsymbol{\psi} = [\psi_1, \psi_2, \ldots, \psi_n]^{\mathrm{T}}$, etc.

The integrals represented by (4.10) can be evaluated analytically as shown by Ingham & Kelmanson (1984). Equation (4.11) represents n equations in $4n$ unknowns and normally there will be only $2n$ boundary conditions given by the problem. Thus use is made of the equation

$$\nabla^2\psi = -\omega, \tag{4.12}$$

to provide a further n equations,

$$\boldsymbol{J\omega}+\boldsymbol{K\omega'}=\boldsymbol{0}, \tag{4.13}$$

where the matrices $\boldsymbol{J}$ and $\boldsymbol{K}$ are the same as those in (4.10) and the analysis used to obtain this equation is similar to that used to derive (4.11).

Because of the re-entrant corner singularity at S, numerical results using the above formulae are very inaccurate (see Ingham & Kelmanson 1984), and we subtract the singularity part of the stream function to leave a smooth solution, taking

$$\psi = g+\chi, \tag{4.14}$$

with

$$g(r,\theta) = r^{\frac{3}{2}}(\tfrac{1}{3}A^*\cos\tfrac{3}{2}\theta + A^*\cos\tfrac{1}{2}\theta) + r^2C^*(1-\cos 2\theta), \tag{4.15}$$

where χ satisfies (4.1) and contains no singular terms. The problem is then redefined and solved in terms of χ with g being added once χ has been found. The values of the constants A^* and C^* are unknown, and must be calculated as part of the solution. This normally gives $2n+2$ unknowns with $2n$ equations and to close the system the unknowns in terms of χ nearest the singular point S are set to zero and said to be dominated by the singularity. By numbering the boundary segments from the singular point S in an anticlockwise fashion so that the boundary segments 1 and n are those which contain points $(0, 1)$ and $(0-, 0)$, respectively, since ψ and ψ' are the specified boundary conditions, this means that the variables ω_1 and ω_2 are set to zero.

Care must be taken to add the singular terms as part of the global solution, as adding them to the boundary solution leads to instability. The asymptotic expansions of boundary conditions (2.14a) and (2.14b) are used at $x = x_L < 0$ and $x = x_R > 0$ to increase the accuracy of the boundary conditions where x_L and x_R are the values of x at which (2.14a) and (2.14b) are applied, respectively.

5. The laboratory experiments

A series of laboratory experiments has been carried out as a test of the numerical solutions and as a means of distinguishing these from other solutions obtained for this flow. The cascade, somewhat like a plane rake or comb, was cut from a thin aluminium plate with square-ended teeth of uniform width 0.01 m separated by uniform gaps of 0.01 m. The spine of the comb was supported vertically and at right angles to the axis of the tank on a light trolley which could be driven along the tank at steady speed by a 6 V permanent magnet d.c. motor with pulse width modulated controller. The tank was of length 1 m, width 0.15 m, and was filled to a depth of approximately 0.12 m using either water or ethylene glycol, thereby providing both a range of driving speeds and of liquid viscosity, and a corresponding range of Reynolds numbers of the motion.

In practice the range of R available between the minimum voltage for steady motion and that at which the first signal of unsteadiness appeared in the flow is about 0.1 to 25. Only the teeth of the comb project into the liquid, reaching to approximately 0.005 m above the lower boundary, while there is a clearance of approximately 0.01 m on each side between tank wall and neighbouring tooth. Thus, there are seven teeth across the tank making up a plane cascade with 50% blockage, and the flow is recorded about the middle three teeth at midheight in the tank as the cascade is travelling at uniform speed in the centre of its run.

Flow past the comb teeth is visualized by seeding the entire fluid with small polyester spheres used in Dulux emulsion paints. These spheres are coated with titanium oxide and have mean diameter 17 μm, 71% of mass in the range 10.5 to

23.7 μm, and 96% of mass in the range 1.3 to 33.7 μm; they settle out slowly, but can be stirred back into suspension before each group of runs to provide a good distribution after the stirring motion has decayed. A decay time of about twenty minutes was left between runs to ensure that residual motion in the tank had been reduced to a low level. These small white spheres are illuminated using light from good quality projectors with slits in their focal planes focused into thin horizontal sheets of light of between 0.002 and 0.005 m thickness in the working section. Two opposed projectors were required to obtain records adequately illuminated both upstream and downstream of the cascade, and these were directed at roughly 45° towards the cascade from either side of the tank with one projector upstream and one downstream at the moment of record. The recording camera was mounted on the trolley and looked vertically down the downstream face of the centre tooth, and the thickness of light sheet in the working section was chosen to illuminate just sufficient particles for a clear record in an exposure time of between 4 and 15 s according to the speed at which the cascade travelled. Care was needed to minimize glare in the strong illumination, and all metal surfaces were painted matt black.

The platform was driven by a rubber covered roller on square-section aluminium tubes which could be levelled and were attached above the sides of the tank. At low speeds there was a small tendency towards oscillations of small amplitude and relatively high frequency. These are, however, very clearly visible in the photographic record when present and it is apparent when they are contaminating the record.

6. Results and discussion

Numerical results were obtained using the modified central-difference scheme for $\beta(=H_C/H_W)=2, 0\leqslant R\leqslant 500, h=k=\frac{1}{10}, \frac{1}{20}, \frac{1}{30}, \frac{1}{40}, \frac{1}{50}$ and $\frac{1}{60}$, and for several positions at which the infinity boundary conditions were specified. One of the main aims of the present study is to find an accurate numerical method for solving the flow through a cascade with boundary singularities, and we have computed only the case $\beta=2$ which corresponds to a relatively large blockage ratio ($1/\beta=0.5$). It is hoped that other blockage ratios will be considered in future work in order to investigate the existing theories, numerical and experimental results.

At $R=0$ results were obtained by the finite-difference method, using both methods I and II to deal with the singularity at the point S, and the BEM. In this case we pay particular attention to the constant A^* which occurs in the expansions (3.4) and (3.5), since the first term of (3.5) is the dominant one which gives the vorticity in the neighbourhood of S. Values of A^* were 2.452, 2.490, 2.503 with mesh sizes $h=k=\frac{1}{20}, \frac{1}{30}, \frac{1}{40}$, respectively, using method II; and 2.516, 2.518, 2.519 with the mesh sizes $\frac{1}{10}, \frac{1}{20}, \frac{1}{40}$ by using the BEM. The corresponding repeated h^2-extrapolation values for A^* obtained by method II and the BEM are both 2.52. All the results of the BEM were found to be graphically indistinguishable from the results obtained using method II as $h, k\to 0$. The results of method I, however, did not appear to be consistent with those of method II and the BEM. The numerical solutions given by method I suggest that the vorticity $\omega(0, 1-k)$ increases indefinitely as $h, k\to 0$, whereas expansion (3.5) indicates that the vorticity at this point should be bounded as $h, k\to 0$.

The inaccuracy in method I can be explained as follows. From this method,

$$\omega(0,1+k)=\tfrac{1}{4}\{\omega(-h,1)+\omega(h,1)+\omega(h,1+2k)+\omega(-h,1+2k)\}, \tag{6.1}$$

hence

$$|\omega(0,1+k)| \leqslant \max\{|\omega(-h,1)|, |\omega(h,1)|, |\omega(h,1+2k)|, |\omega(-h,1+2k)|\}. \tag{6.2}$$

From (3.5), however, we have

$$\omega \sim -2A^* r^{-\frac{1}{2}} \cos(\tfrac{1}{2}\theta), \tag{6.3}$$

and for $h = k$

$$|\omega(0,1+k)| > \max\{|\omega(-h,1)|, |\omega(h,1)|, |\omega(h,1+2k)|, |\omega(-h,1+2k)|\}. \tag{6.4}$$

Hence from (6.2) and (6.4) we have a contradiction. Thus substantial errors arise in method I from the evaluation of $\omega(0,1+k)$, even for small h, k. Although method I has been used successfully by some authors, it is clear that inaccuracies arise when using the method for $R = 0$; indeed, further tests over a wide range of Reynolds numbers have shown similar conclusions. The inaccuracies in method I near the point S will introduce unacceptable error into such quantities as drag coefficient and length of attached flow. In this paper method II has been used in all calculations.

As method II yielded a satisfactory result for $R = 0$, further investigations using this method are given also for both intermediate and high values of the Reynolds number. For all small and intermediate Reynolds numbers, solutions were obtained with $h = k = \frac{1}{10}, \frac{1}{20}, \frac{1}{30}$ and $\frac{1}{40}$. At larger values of the Reynolds numbers, calculations were performed also with $h = k = \frac{1}{50}$ and $\frac{1}{60}$ in order to ensure accurate results, but these calculations are very expensive in computer time.

There are several ways of calculating pressure in the flow field and on the plate surface. In (x, y)-coordinates the Navier–Stokes equations of motion can be written in non-dimensional form,

$$\frac{\partial p}{\partial x} = \frac{2}{R}\nabla^2 u - \left(u\frac{\partial u}{\partial x} + v\frac{\partial u}{\partial y}\right), \tag{6.5}$$

$$\frac{\partial p}{\partial y} = \frac{2}{R}\nabla^2 v - \left(u\frac{\partial v}{\partial x} + v\frac{\partial v}{\partial y}\right). \tag{6.6}$$

On the x-axis, $v = 0$ and therefore (6.5) becomes

$$\frac{\partial p}{\partial x} = -\frac{2}{R}\frac{\partial \omega}{\partial y} - u\frac{\partial u}{\partial x}, \tag{6.7}$$

which on integration gives

$$p(0-,0) = -\frac{2}{R}\int_{-\infty}^{0} \frac{\partial \omega}{\partial y}(x,0)\,dx - \tfrac{1}{2}u^2(0-,0) + \tfrac{1}{2}u^2(-\infty,0). \tag{6.8}$$

Using (2.11a), (2.12a) and (2.13a) we have

$$\int_{-\infty}^{x_L} \frac{\partial \omega}{\partial y}(x,0)\,dx \sim -\frac{1}{\alpha_1}\frac{\partial \omega}{\partial y}(x_L,0), \tag{6.9}$$

and since $u(-\infty,0) = 1$ and $u(0-,0) = 0$ we obtain

$$p(0-,0) \sim -\frac{2}{R}\int_{x_L}^{0} \frac{\partial \omega}{\partial y}(x,0)\,dx + \frac{2}{\alpha_1 R}\frac{\partial \omega}{\partial y}(x_L,0) + \tfrac{1}{2}. \tag{6.10}$$

Along the plate OS, $u = 0$ and $v = 0$ and therefore (6.6) becomes

$$\frac{\partial p}{\partial y} = \frac{2}{R}\frac{\partial \omega}{\partial x}, \tag{6.11}$$

which on integration gives

$$p(0-,y) = p(0-,0)+\frac{2}{R}\int_0^y \frac{\partial\omega}{\partial x}(0-,y)\,\mathrm{d}y. \tag{6.12}$$

In a similar manner, the pressure on the downstream surface reduces to

$$p(0+,y) = p(0+,0)+\frac{2}{R}\int_0^y \frac{\partial\omega}{\partial x}(0+,y)\,\mathrm{d}y, \tag{6.13}$$

where

$$p(0+,0) \sim \frac{2}{R}\int_0^{x_R} \frac{\partial\omega}{\partial y}(x,0)\,\mathrm{d}x+\frac{2}{\alpha_1^* R}\frac{\partial\omega}{\partial y}(x_R,0)+\tfrac{1}{2}. \tag{6.14}$$

Formulae (6.12) and (6.13) are evaluated numerically using Simpson's rule. The drag D on the plate may be expressed as

$$D = \rho U^2 H_W C_D \tag{6.15}$$

in terms of the non-dimensional drag coefficient C_D, which can be evaluated from

$$C_D = \int_0^1 [p(0-,y)-p(0+,y)]\,\mathrm{d}y. \tag{6.16}$$

Integrating by parts,

$$C_D = p(0-,0)-p(0+,0)+\frac{2}{R}\int_0^1 (1-y)\frac{\partial}{\partial x}(\omega(0-,y)-\omega(0+,y))\,\mathrm{d}y. \tag{6.17}$$

Because of the singularity at S, where the vorticity and vorticity gradient are unbounded, a special treatment is needed in the neighbourhood of the singularity. Using Moffatt's (1964) expansion, a modified formula can be obtained:

$$C_D = p(0-,0)-p(0+,0)+\frac{2}{R}\int_0^{1-h} (1-y)\frac{\partial}{\partial x}(\omega(0-,y)-\omega(0+,y))\,\mathrm{d}y+\frac{8A^*h^{\frac{1}{2}}}{R}. \tag{6.18}$$

In order to check the accuracy, the following alternative formula for C_D may be used:

$$C_D = h(p(0-,1-h)-p(0+,1-h))+\int_0^{1-h} [p(0-,y)-p(0+,y)]\,\mathrm{d}y+\frac{8A^*h^{\frac{1}{2}}}{R}. \tag{6.19}$$

Evaluations of C_D using these two methods gives a consistency check on the solution. Two sets of solutions for C_D were obtained and found to be in very good agreement.

The upstream and downstream positions at which the infinity boundary conditions were applied, x_L and ξ_R, were varied for each Reynolds number. Values of x_L and ξ_R have been taken sufficiently large so that any further increase produces only a negligible change in all flow quantities evaluated when using the finest mesh and in the extrapolated results. In practice it was found that the results for the wake length L were not too sensitive to the exact location ξ_R. For example, in the case $R = 100$, the results for L using $(x_L, \xi_R) = (-2,4)$, $(-2,6)$ and $(-3,6)$ were in very good agreement. However, the results for the drag coefficients C_D were found to be more sensitive to the effects of boundary locations and in the above example they can be estimated correctly only to within about 10% for the smaller region.

Figure 3 shows the variation of vorticity on the upstream and downstream faces of the plate using several mesh sizes for $R = 10$, 100 and 500. It is seen that as the mesh size tends to zero the results appear to be converging to a solution, although

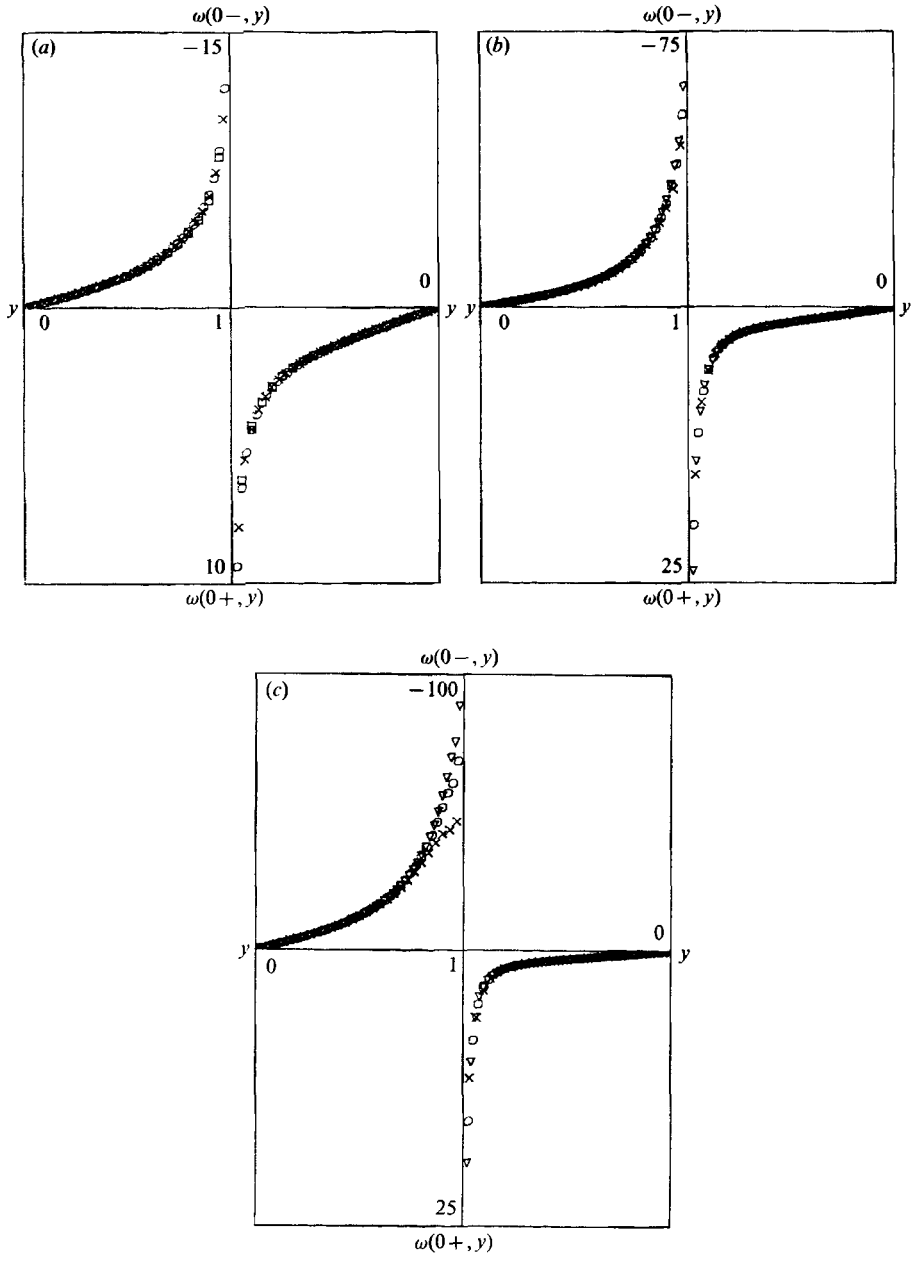

FIGURE 3. Mesh size influence on the vorticity distribution on the surface of the plate: (*a*) $R = 10$, with $h = k = \frac{1}{20}, \frac{1}{30}$, and $\frac{1}{40}$; (*b*) $R = 100$, (*c*) $R = 500$, with $h = k = \frac{1}{30}, \frac{1}{40}$ and $\frac{1}{50}$. ∇, $\frac{1}{50}$; $\bigcirc$, $\frac{1}{40}$; $\times$, $\frac{1}{30}$; $\square$, $\frac{1}{20}$. These results were obtained by method II.

FIGURE 4 (*a–d*). Streamlines for (*a*) $R = 1$ (the values of stream functions, starting from the top, are $\psi = 2.0, 1.6, 0.8, 0.4, 0.2, 0.1, 0.02, 0.002$; enclosed stream functions, starting from the centre, are $\psi = -0.0004, 0$); (*b*) $R = 10$ (the values of stream functions, starting from the top, are $\psi = 2.0, 1.6, 0.8, 0.4, 0.2, 0.1, 0.02$; enclosed streamlines, starting from the centre, are $\psi = -0.06, -0.04, -0.02, 0$); (*c*) $R = 100$; (*d*) $R = 500$ (in the last two cases, the values of stream functions, starting from the top, are $\psi = 2.0, 1.6, 0.8, 0.4, 0.2, 0.1, 0.02$; enclosed streamlines, starting from the centre, are $\psi = -0.3, -0.2, -0.1, 0$). (*e–h*) Equivorticity lines for (*e*) $R = 1$; (*f*) 10; (*g*) 100; (*h*) 500.

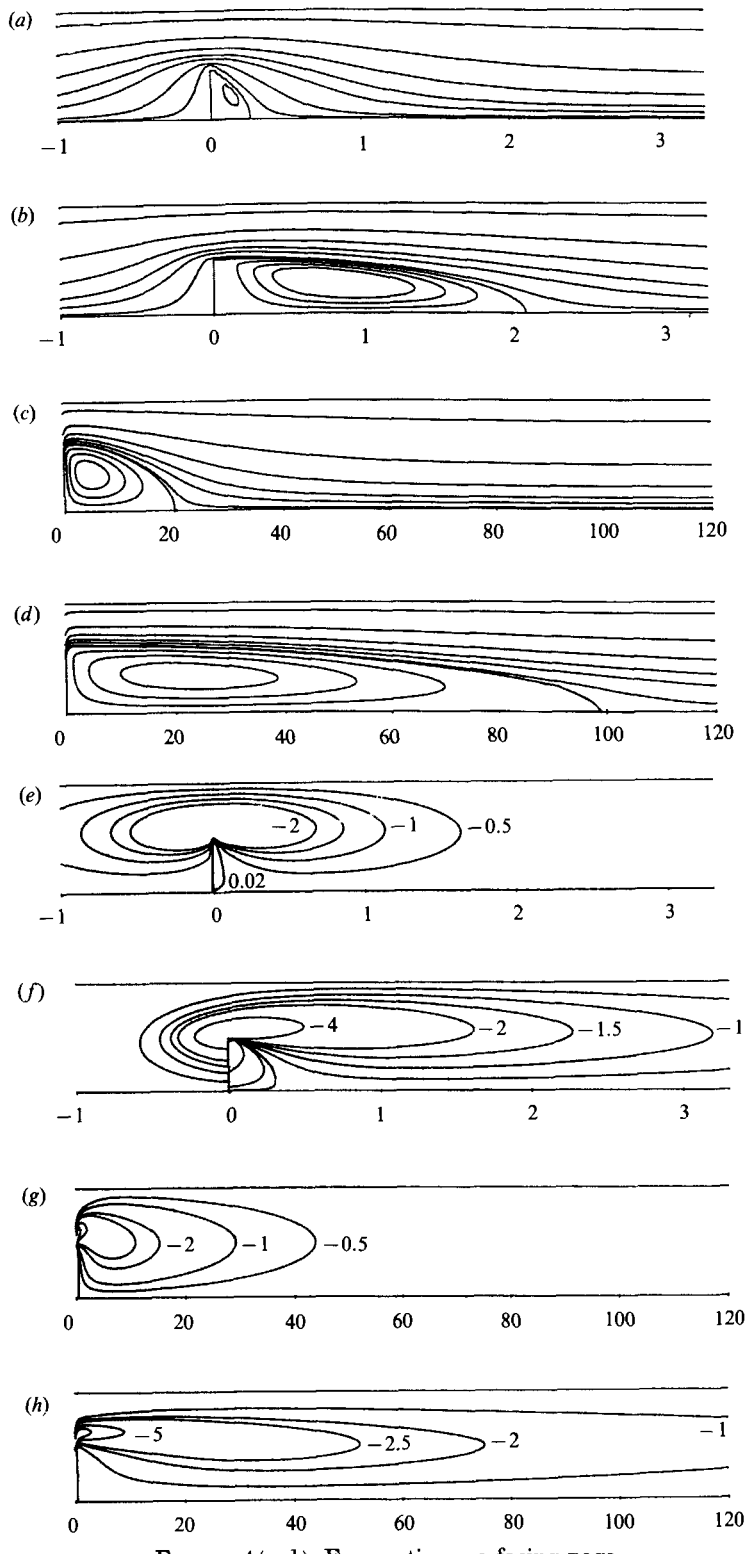

FIGURE 4(*a–h*). For caption see facing page.

some inaccuracies still exist on the upstream face near the singularity especially at the larger values of Reynolds number.

The flow streamlines and equivorticity lines for $R = 1$, 10, 100 and 500 are presented in figure 4, and the vorticity on the surface of the plate is shown in figure 5 using the results on the finest grids. It is noted that the magnitudes of the vorticity gradients in the present work are similar to those obtained by Fornberg (1980, 1985) when solving the steady flow past a circular cylinder.

A series of experiments has been carried out in which the trolley (and hence the cascade) is initially accelerated rapidly to uniform speed U which is then maintained over the greater part of the tank, and is finally accelerated negatively to rest. The range of velocities (0.0005 to 0.5 m s^{-1}) and length of tank used are such that the flow has become essentially steady before the point at which it is photographed. Figure 6 shows a set of 4 s time exposures showing the motion of the polystyrene marker spheres in a thin horizontal illuminated section at mid-level in the tank. The cases illustrated are (*a*) for $R = 4.0$ in ethylene glycol, (*b*) for $R = 8.3$ in ethylene glycol, (*c*) for $R = 17.9$ in water, and (*d*) for $R = 22.2$ in ethylene glycol. To the left of each experimental photograph is a streamline field obtained numerically for that Reynolds number, and it may be seen that the numerical and experimental realizations are in excellent broad agreement despite additional constraints in the laboratory experiment due to the side walls and floor of the channel and to the free surface of the liquid. The region of flow shown in the photographs is 0.04 m from the sidewalls and 0.06 m from both the free surface and bottom of the tank, and the character of the flow (which is from left to right relative to the cascade plates) is shown clearly. In each case, the flow separates from the edges of the plates forming an attached bubble consisting of a vortex pair. The diagonal pattern is caused by the use of light sources slanting rearwards to the left and forwards to the right; these produce bright diagonal bands where the marker particles are illuminated by both sources, and darker bands of roughly half the intensity where one beam is obstructed by a tooth of the cascade. However, the illumination is sufficient to resolve the pattern of flow. A better system of illumination will be used in future experiments.

In order to cover as wide a range of flows as possible and to show that the scaling used has been appropriate, the cascade was run in water and in ethylene glycol over the Reynolds-number range of about 0.1 to 22. These limits were imposed by the format of the experiment, as below 0.1 it proved difficult to drive the trolley smoothly with the motor gearbox configuration available, while above 22 the flow started to show signs of unsteadiness. The full set of experimental results is presented in figure 7, in which the non-dimensional length of the attached flow behind cascade teeth measured in terms of the width of a tooth is plotted against Reynolds number. Measurements in water are shown by stars (*), and those in ethylene glycol by triangles ($\triangle$). It is observed that as the Reynolds number increases so does the length of the recirculating eddy behind the plate and this is in agreement with the numerical results presented in figure 4.

Table 1 gives the eddy length, L, as obtained by the numerical calculations for different mesh sizes and those obtained using repeated h^2-extrapolations on consecutive mesh sizes for several values of the Reynolds number, whilst figure 8 shows the variation of the length of the eddy at Reynolds numbers 100, 200 and 500 as functions of h and h^2. It is observed for $R \leqslant 200$ that h^2-extrapolation of the results is justified, but for $R = 500$ it is not. Although the basic finite-difference scheme used is second-order accurate in the limit of infinitesimal steps, if the steps used are not small compared with the inverse of the Reynolds number, then the 'upwinding'

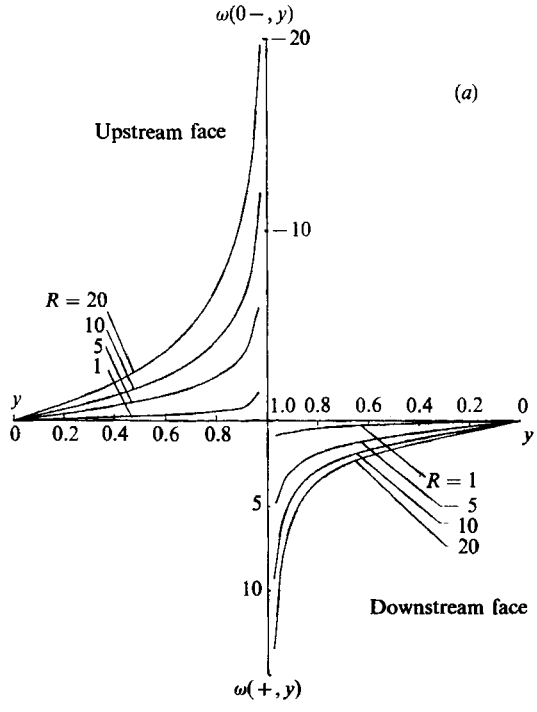

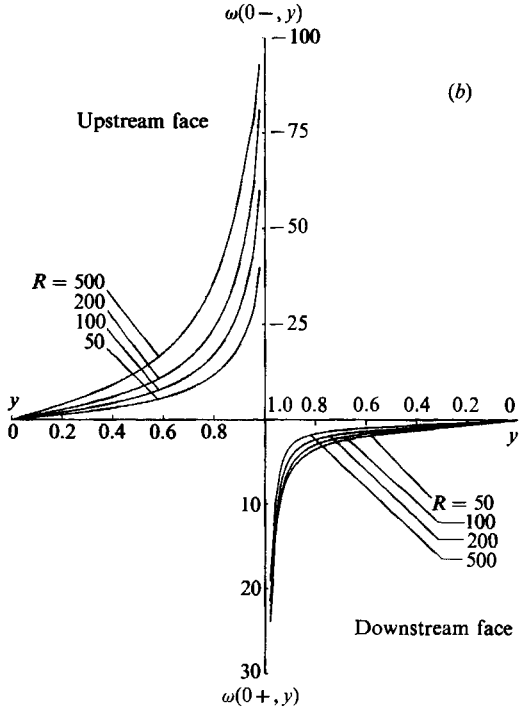

FIGURE 5. Vorticity distribution on the surface of the plate for (*a*) $R = 1$, 5, 10, and 20; (*b*) $R = 50$, 100, 200, 500.

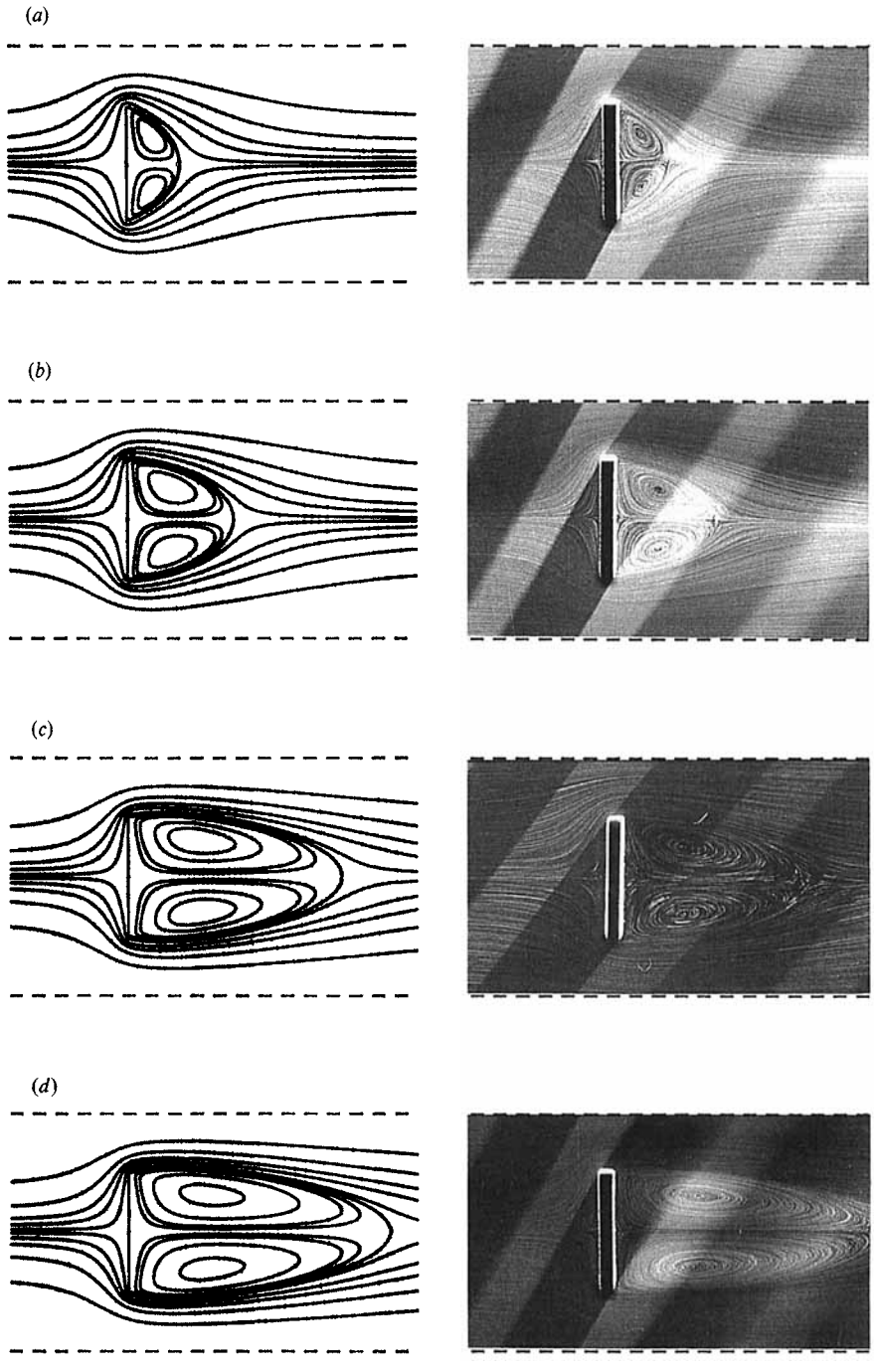

FIGURE 6. Comparison of calculated and experimental streamlines for (*a*) $R = 4.0$; (*b*) 8.3; (*c*) 17.9; (*d*) 22.2. The experimental results of (*a*, *b*, *d*) were obtained by using ethylene glycol whilst for (*c*) pure water was used.

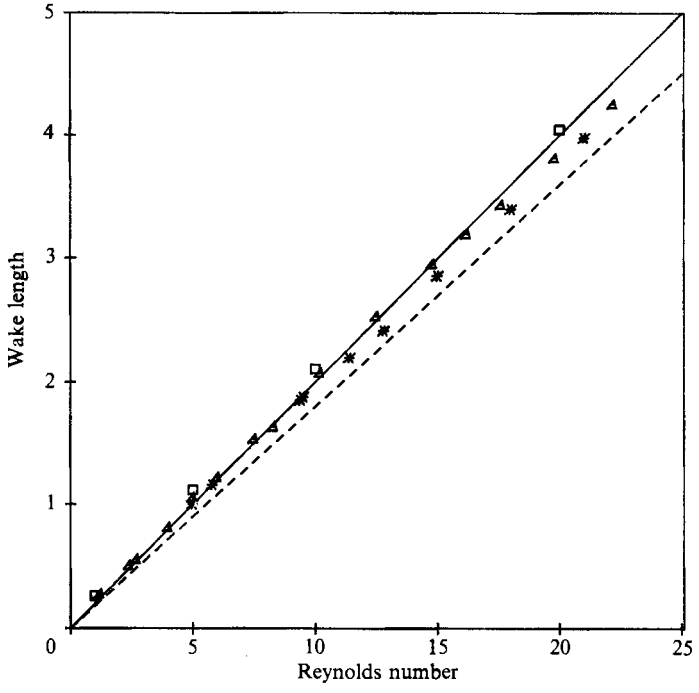

FIGURE 7. Comparison of theoretical, numerical and experimental results for non-dimensional eddy length against Reynolds number. □, Present numerical results; △, experimental results in ethylene glycol; *, experimental results in pure water; ——, Smith (1985*a*); – – –, Milos & Acrivos (1986), Milos *et al.* (1987).

R	1	5	10	20	50	100	200	500
x_L	−10	−10	−6	−6	−6	−2	−2	−2
ξ_R	2	2	4	4	4	6	6	6
$h = k = \frac{1}{10}$	0.234	1.085	2.049	3.898	—	—	—	—
$h = k = \frac{1}{20}$	0.258	1.107	2.092	3.998	9.728	19.09	36.09	82.22
$h = k = \frac{1}{30}$	0.259	1.113	2.101	4.024	9.882	19.75	38.51	88.73
$h = k = \frac{1}{40}$	0.260	1.116	2.104	4.034	9.958	20.02	39.77	93.59
$h = k = \frac{1}{50}$	—	—	—	—	9.998	20.14	40.43	97.07
$h = k = \frac{1}{60}$	—	—	—	—	—	—	40.77	99.40
Extrapolation	0.261	1.119	2.108	4.048	10.078	20.36	41.26	104.96
Smith (1985*a*)	0.20	1.00	2.00	4.00	10.00	20.00	40.00	100.00

TABLE 1. Values of the attached eddy length L.

amounts to inclusion of artificial viscosity which cannot be separated from the real viscosity. Thus the extrapolated results at $R = 500$ should be used with caution.

The results for the eddy length L, which are given in table 1, suggest that for large Reynolds numbers

$$L \sim 0.21R, \tag{6.20}$$

whereas the theoretical results on the related problem of Smith (1985*a*) gives

$$L \sim 0.20R. \tag{6.21}$$

It should be noted that the laboratory measurements do exhibit some scatter and

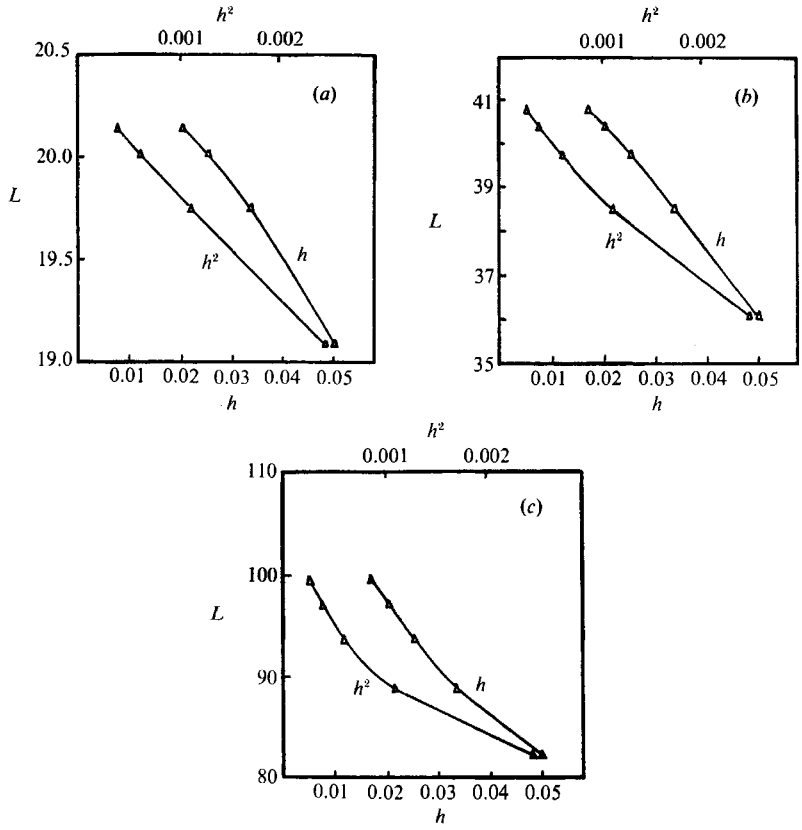

FIGURE 8. The variation of the eddy length as a function of h and h^2 for (*a*) $R = 100$; (*b*) 200; (*c*) 500.

lie systematically under the numerical and theoretical solutions, but taking account of the difficulty in identifying the stagnation point marking the end of the attached flow our laboratory results provide striking support for our numerical solution. Thus both our numerical and experimental results provide support for an approximately linear dependence of relative attached flow length on Reynolds number, although it may be noted that the dependence is not quite linear at low Reynolds numbers. The final comparison made in figure 7 is with the numerical results of Milos & Acrivos (1986) and Milos *et al.* (1987) (broken line) who studied the related problems of laminar flow over a backward-facing step on one side of a two-dimensional channel. From their boundary-layer solutions (1986) and Navier–Stokes solutions (1987), we find the following formula:

$$L \sim 0.18R, \tag{6.22}$$

in the present notation, and it is observed from figure 7 that the agreement with the present numerical and experimental work is favourable.

Figure 9 shows the h^2-extrapolated values of the x- and y-components of velocity at $x = 0$, $u(0, y)$ and $v(0, y)$ respectively, as a function of y at Reynolds numbers 1, 10, 100 and 500. It is observed that as the Reynolds number increases the x-component of velocity approaches the asymptotic profile used by Smith (1985*a*) but the y-component of the velocity does not. In fact as the Reynolds number increases this component of velocity increases, rather than tending to zero, which results in $(\partial v/\partial y)(0, y)$ increasing over much of the range $1 < y < 2$. From the continuity equation we deduce that $(\partial/\partial x)\, u(0, y)$ does not tend to zero, which is again a

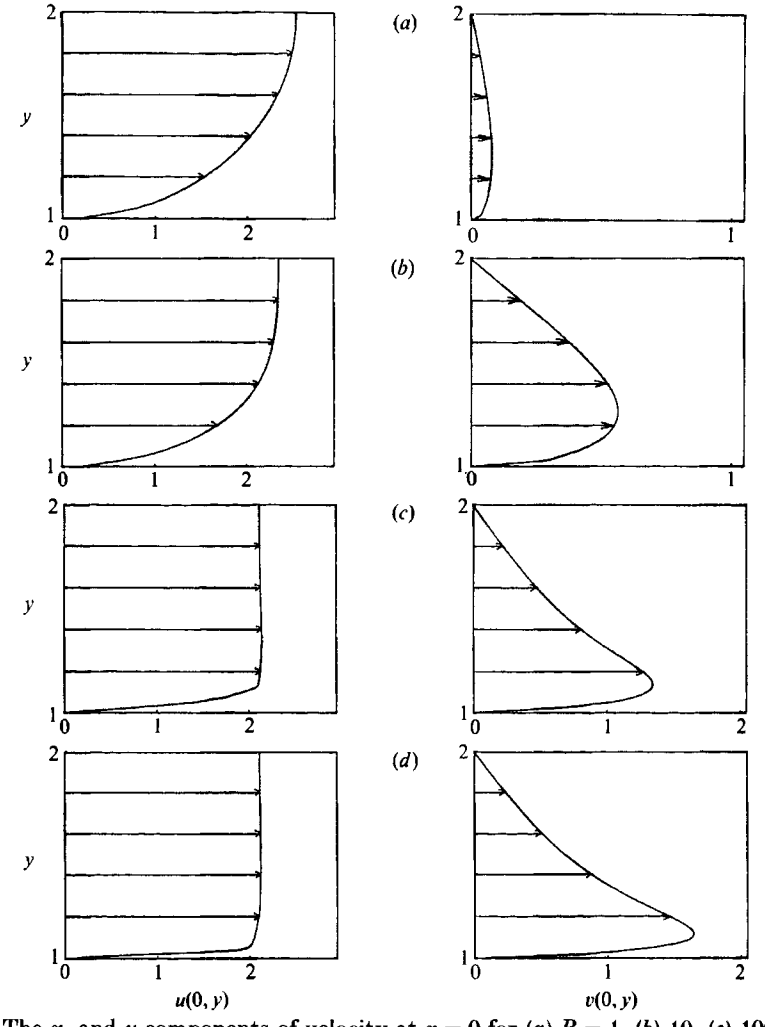

FIGURE 9. The x- and y-components of velocity at $x = 0$ for (*a*) $R = 1$, (*b*) 10, (*c*) 100 and (*d*) 500.

R	1	5	10	20	50	100	200	500
x_L	−10	−10	−6	−6	−6	−2	−2	−2
ξ_R	2	2	4	4	4	6	6	6
$h = k = \frac{1}{10}$	17.70	4.177	2.808	2.292	—	—	—	—
$h = k = \frac{1}{20}$	17.91	4.213	2.815	2.265	2.083	2.200	2.648	2.729
$h = k = \frac{1}{30}$	17.99	4.228	2.820	2.261	2.055	2.092	2.335	2.595
$h = k = \frac{1}{40}$	18.03	4.236	2.823	2.260	2.044	2.055	2.206	2.495
$h = k = \frac{1}{50}$	—	—	—	—	2.036	2.036	2.144	2.416
$h = k = \frac{1}{60}$	—	—	—	—	—	—	2.106	2.344
Extrapolation	18.11	4.252	2.830	2.260	2.012	1.996	1.989	1.973

TABLE 2. Values of the drag coefficient C_D.

boundary condition frequently used when solving the related problems. The generation of the non-zero y-component of velocity at $x = 0$ is not unexpected because as the Reynolds number increases the flow does not know of the existence of the plates until it gets quite close to them. This results in a large y-component of the velocity near the upstream surface of the plates, see figure 4(*a*), and this flow has

to be brought to rest at $y = 2$. Thus the good agreement obtained between the present investigation and those of Smith, Acrivos etc. could not be foreseen as the problems studied are quite distinct.

Results for the drag coefficient derived from (6.18) are presented in table 2. It may be seen that at small values of R the values of C_D can be predicted very accurately, whereas at the large values, say 200 and 500, C_D can be estimated only to within a few per cent. One reason is that inaccuracies occur on the upstream face near the singularity point, S, at larger values of R, as may be seen from figure 3.

The authors would like to thank Professor F. T. Smith for bringing this problem to their attention and for the numerous constructive comments he has made on several aspects of the work. Further the paper has been substantially improved by the comments of the referees. Also Terry Long of the Monash Geophysical Fluid Dynamics Laboratory has made a significant contribution to the experimental side of this work and it is a pleasure to place on record our high regard for his resourcefulness and support. One of the authors (T.T.) acknowledges with thanks the financial support provided by the University of Leeds.

REFERENCES

Acrivos, A., Leal, L. G., Snowden, D. D. & Pan, F. 1968 *J. Fluid Mech.* **34**, 25.

Acrivos, A. & Schrader, M. L. 1982 *Phys. Fluids* **25**, 923.

Acrivos, A., Snowden, D. D., Grove, A. S. & Peterson, E. E. 1965 *J. Fluid Mech.* **21**, 737.

Badr, H., Dennis, S. C. R., Bades, S. & Smith, F. T. 1985 *J. Fluid Mech.* **156**, 63.

Bramley, J. S. & Dennis, S. C. R. 1982 *8th Intl Conf. on Numerical Methods in Fluid Dynamics.* Lecture Notes in Physics, vol. 170, p. 155. Springer.

Bramley, J. S. & Dennis, S. C. R. 1984 *Computers Fluids* **12**, 339.

Castro, I. P., Cliffe, K. A. & Norgett, M. J. 1982 *Intl J. Numer. Meth. Fluids* **1**, 3.

Castro, I. P. & Jones, J. M. 1987 *Intl J. Numer. Meth. Fluids* **7**, 793.

Dennis, S. C. R. & Hudson, J. D. 1978 In *Proc. 1st Conf. Num. Meth. Laminar and Turbulent Flow*, p. 69. London: Pentech.

Dennis, S. C. R. & Hudson, J. D. 1980 *J. Inst. Maths Aplics.* **26**, 369.

Dennis, S. C. R. & Smith, F. T. 1980 *Proc. R. Soc. Lond.* A **372**, 393.

Fornberg, B. 1980 *J. Fluid Mech.* **97**, 819.

Fornberg, B. 1985 *J. Comput. Phys.* **61**, 297.

Holdstein, H. & Paddon, D. J. 1981 *J. Non-Newtonian Fluid Mech.* **8**, 81.

Hudson, J. D. & Dennis, S. C. R. 1985 *J. Fluid Mech.* **160**, 369.

Ingham, D. B. 1983 *Computers Fluids* **11**, 351.

Ingham, D. B. & Kelmanson, M. A. 1984 *Boundary Integral Equation Analysis of Singular, Potential and Biharmonic Problems.* Springer.

Kirchhoff, G. 1869 *J. Reine Angew. Math.* **70**, 289.

Milos, F. T. & Acrivos, A. 1986 *Phys. Fluids* **29**, 1353.

Milos. F. T., Acrivos, A. & Kim, J. 1987 *Phys. Fluids* **30**, 7.

Moffatt, H. K. 1964 *J. Fluid Mech.* **18**, 1.

Peregrine, D. H. 1985 *J. Fluid Mech.* **157**, 493.

Prandtl, L. & Tietjens, O. G. 1934 *Applied Hydro- and Aeromechanics.* McGraw-Hill.

Smith, F. T. 1979 *J. Fluid Mech.* **92**, 171.

Smith, F. T. 1985*a* *J. Maths Phys. Sciences* **19**, 1. (Previously published for limited circulation as United Tech. Res. Centre internal report UTRC-83-13.)

Smith, F. T. 1985*b* *J. Fluid Mech.* **155**, 175.

Wilson, S. D. R. 1969 *J. Fluid Mech.* **38**, 793.

Woods, L. C. 1954 *Aeronaut. Q.* **5**, 176.